Macromolecules

pubs.acs.org/Macromolecules Article

Polymer-Assisted Condensation: A Mechanism for Heterochromatin Formation and Epigenetic Memory

Jens-Uwe Sommer,* Holger Merlitz, and Helmut Schiessel

Cite This: *Macromolecules* 2022, 55, 4841−4851 Read Online

ACCESS | Metrics & More | Article Recommendations

ABSTRACT: We consider the formation of droplets from a 2-component liquid mixture induced by a large polymer chain that has preferential attraction to one of the components. We assume that the liquid mixture is in a fully miscible state, but far above the critical interaction limit of the two species. We show that the polymer coil acts as a chemical potential trap, which can shift the mixture inside the polymer volume into the partially miscible state and thus triggers the formation of a polymer-bound droplet of the preferred solvent phase, which we denote as polymer-assisted condensation (PAC). We propose a mean-field model which can predict the essential features of PAC including the phase diagram, and we perform molecular dynamics simulations to show that the predicted phase behavior is robust against fluctuation effects. The properties of PAC make it an ideal candidate to understand the formation of biomolecular condensates inside the cell nucleus, such as those formed by the protein heterochromatin 1 (HP1). We propose that such droplets organize the spatial structure of chromatin into hetero- and euchromatin and their predicted stability with respect to the chromatin-HP1-interaction ensures the propagation of epigenetic information through the cell generations.

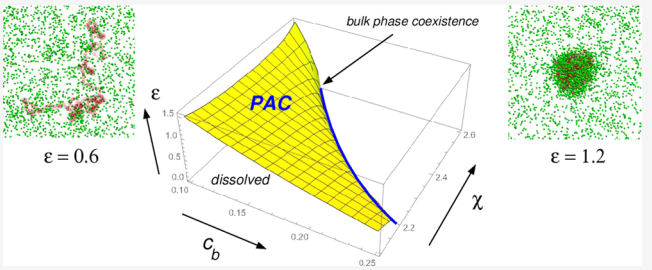

1. INTRODUCTION

The interpretation of processes in living cells with the toolbox of polymer physics is increasingly turning into a new paradigm of life sciences. A prominent example is cell division, in which typically meters of entangled DNA molecules have to be separated and precisely distributed between the two daughter cells. Recent work suggests that the underlying mechanism involves the formation of nonconcatenated DNA loops produced by loop extrusion complexes.[1,2] Other loop extruders organize the spatial structure of DNA in interphase.[3,4] These observations, in turn, have inspired new polymer physics studies on solutions of nonconcatenated polymer rings[5−13] (see also ref 14).

The current work is inspired by a problem encountered by cells after cell division, which we speculate also uses polymer physics, namely the recovery of lost epigenetic information in the daughter cells. Epigenetics is defined as modifications of the functions of genes that are stable and inheritable through cell division (see, for example ref 15). As all cells contain the same genes, epigenetics defines the cell type. On a molecular level, epigenetic information is stored through covalent modifications of histone proteins where specific amino acids carry epigenetic tags in the form of, for example, methylations and acetylations.[15] Histone proteins are associated with the DNA in nucleosomes, DNA−protein complexes, where roughly a persistence length of DNA, about 150 base pairs (bp), are wrapped around an octamer of histone proteins.[16,17] About 3/4 of human DNA is sequestered this way. An important epigenetic mark is H3K9me3, the trimethylation of lysine 9 on histone H3. Nucleosomes that carry this tag are part of heterochromatin,[15] a denser and less accessible part of chromatin, as compared to the more open euchromatin, in which most of the actively transcribed genes are located.

During DNA duplication the nucleosomes are randomly distributed between the DNA molecules of the two daughter cells,[18] and the missing nucleosomes are then refilled by new nucleosomes. As only the old nucleosomes carry epigenetic marks, this process causes the information to be "diluted" by a factor two. The challenge is now to put the marks back onto the new nucleosomes. For the case of the H3K9me3 tags, blocks of nucleosomes carrying this tag (with median length of about 50 nucleosomes in humans[19]), alternate with blocks without this tag.[20] It is not known how enzymes in the daughter cell reliably and robustly put the lost H3K9me3 marks back to the heterochromatic blocks. Models put forward to describe heterochromatin formation and self-maintenance typically take a one-dimensional view in which heterochromatic marks spread along the nucleosome chain, stopped by

Received: February 1, 2022
Revised: May 9, 2022
Published: May 25, 2022

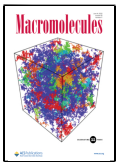

barrier insulators at the borders to euchromatin.[19,21] However, this view neglects the fact that chromatin is a polymer, randomly folded in three dimensions so that barrier elements alone might not be sufficient to contain the spread of heterochromatin. Another mechanism is needed that isolates euchromatin from heterochromatin in the three-dimensional context. This mechanism has to overcome various challenges: It needs to provide a physicochemical environment, a "reaction chamber" in which the corresponding enzymes put back the H3K9me3 marks onto the "right" nucleosomes. There needs to be a physical interface defining a boundary between the nucleosomes that belong to the heterogenetic and the euchromatic domains. This physicochemical environment, the heterochromatin-phase, must be robust to a change of the number of epigenetic marks by a factor of 2 and also to flucutations of the concentrations of proteins during the cell-cycle.

We suggest here that such a mechanism requires a particular form of biomolecular condensate, which has meanwhile been observed repeatedly in biological systems.[22] Such droplets, formed typically by protein and RNA molecules, create chemical environments with sharp boundaries against the rest of the cell. It is known for heterochromatin that the protein heterochromatin 1 (HP1) forms droplets at sufficiently high concentrations in vitro,[23,24] which are caused by the attraction between some nonstructured regions in those proteins. In addition, it is known that HP1 binds specifically to the H3K9me3 marks of nucleosomes.[25−27] This suggests that each chromosome with its domains of marked and unmarked nucleosomes acts like a block copolymer at a selective interface between two phases.[28] The blocks containing H3K9me3-nucleosomes would form loops inside the HP1 droplets and the other nucleosomes would loop outside the droplets. Since the boundaries between the two types of nucleosomes would be pinned at the droplet surface, this surface would act as a physical insulator.

If the system is sufficiently robust against changes in parameters, then the daughter cells' chromosomes with their half-diluted marks would still maintain similar configurations regarding loops being in- or outside the droplets after cell division. If the enzyme that puts the marks back to the nucleosomes would only work inside the droplets, then the new nucleosomes inside the heterochromatic blocks would recover the proper H3K9me3 marks, while the nucleosomes in the euchromatic loops outside the condensate would remain unaffected. In fact, the H3K9 methylase Suv39h1 is found associated with HP1.[29,30]

The scenario proposed above requires liquid−liquid phase separation and the formation of protein condensates, which has recently attracted intense research in the physics of life. From the point of view of equilibrium phase transitions, two aspects are puzzling: First, why do condensates form from individually water-soluble components? Second, why do condensates have characteristic sizes, that is, they do not seem to be subject to Ostwald-type ripening? While the first aspect can be explained by attractive interactions between different components,[31] in some cases involving mRNA, the second aspect is often considered as intrinsically non-equilibrium in nature. For the case of HP1 domains, both aspects could be explained at the same time if the condensates require methylated chromatin to form.

In this work we show that binary liquids which are set in a fully miscible state form stable droplets upon weak interactions with long polymers chains, where the size of the condensate is controlled by the size of the collapsed chain or sequences of the chain in equilibrium. We call this mechanism polymer assisted condensation (PAC). We further show that this state is robust with respect to changes of interaction parameters. The latter is important for the function of heterochromatin since after cell-division only half of the methylated nucleosomes are present. Furthermore, our model allows for small changes in the environmental concentration of the condensing protein. While this work is inspired by a concrete biological problem, this paper focuses only on its polymer physics aspect. Specifically, we aim to present a generic model using concepts of polymer physics and reveal its properties analytically in its simplest form, solve it numerically in general, and proof the concept by molecular dynamics simulations.

2. ANALYTICAL MODEL FOR POLYMER-ASSISTED LIQUID−LIQUID PHASE SEPARATION

We start to outline a simple model for the condensation of proteins in the presence of a weakly attractive polymer. Our model is a generic polymer physics model and can be applied to any two-component solution in interaction with a polymer phase. For simplicity we denote the solvent component which selectively interacts with the polymer (cosolute/cosolvent) by HP, and the common solvent as water. We consider the whole polymer chain to be attractive with respect to HP in order to understand the fundamental mechanism of PAC. The model can be readily extended to micelle-like structures formed by copolymers. We further assume a binary interaction between HP and water denoted by χ. We consider a bulk state outside of the polymer region which consists of HP at concentration (volume fraction) c_b in water which is well above the critical point of demixing, $\chi > \chi_c$, but in the mixed state outside of the coexistence region, as indicated by the blue circle on the lhs in Figure 1. This situation is different from that previously considered by Brochard and de Gennes,[32] in which the solvent mixture is above the critical point at which fluctuation effects dominate and metastability does not occur. The essential idea is that the preferential interaction between HP and the polymer, which we call ϵ in the following, shifts the stability of the solution to the condensed state, which in turn is limited by the resulting coil size of the polymer. Our model assumes thermal equilibrium and no active or intrinsically dissipative processes are necessary.

As a starting point, we consider the free energy per volume unit inside the polymer coil in the Flory−Huggins approximation:

$$f_v(c|\phi) = \frac{1}{n}c\ln c + (1-c-\phi)\ln(1-c-\phi) + \chi c(1-c-\phi) - \epsilon\phi c - \mu c + \Pi + f_{el}(\phi) \quad (1)$$

Here, ϕ denotes the monomer volume fraction and c denotes the volume fraction of HP, μ is the chemical potential of the bulk HP, and Π is the osmotic pressure of the bulk phase. Unless stated otherwise, we use k_BT as the unit for the energy, and the volume unit is given by the size of the solvent molecules in the spirit of the Flory−Huggins (FH) lattice model. In general, the size of HP can be n times the size of water. Since we are interested in the general physical understanding of the model we restrict ourselves here to the symmetric case, $n = 1$, which simplifies the analytical arguments substantially. The term $f_{el}(\phi)$ denotes the free energy penalty associated with a swelling of the polymer. Given

https://doi.org/10.1021/acs.macromol.2c00244
Macromolecules 2022, 55, 4841−4851

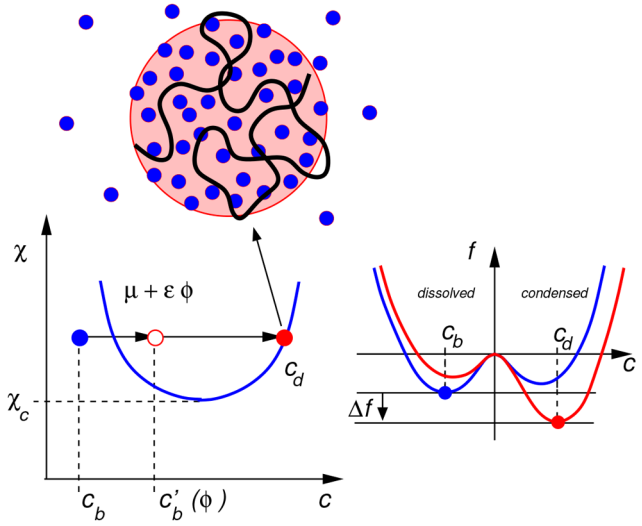

Figure 1. Sketch of the phase diagram of a two-component solution with the HP-concentration given by c (lhs). The coexistence states are indicated by the blue line and the critical interaction parameter is given by χ_c. The blue circle denotes the bulk state with concentration c_b outside of the coexistence region. The presence of the polymer with monomer concentration ϕ shifts the effective chemical potential to a higher value, which can be associated with a virtual increase of the bulk concentration, and gives rise to phase separation of the solution with the stable phase of an HP-polymer-droplet at concentration c_d, shown by the red circle. The rhs illustrates the free energy profile as a function of the concentration: In the bulk the dissolved state is stable and the condensed state is metastable (blue line). The polymer shifts the effective chemical potential (the external field in the context of phase transitions), resulting in a discontinuous transition to the stable condensed state where the dissolved state is metastable (red line). The free energy gain, Δf, due to the interaction with the polymer is given by the arrow.

the elastic free energy per chain according to $F_{el}(\phi) \sim R^2/N \sim (N\phi^2)^{-1/3}$ by using the relation $\phi \sim N/R^3$, where R the radius of gyration of the polymer coil, we obtain for the elastic free energy per volume unit $f_{el}(\phi) = F_{el} \times \phi/N = \alpha\phi^{1/3}N^{-4/3}$ with a numerical prefactor, α, of order unity. We note that the limiting cases of pure solvents (either water or HP in our notation) correspond to good solvents and are given by the limits $c = 0$ and $c = 1 - \phi$, respectively. In these cases eq 1 corresponds to Flory's free energy for a single polymer chain including all virial coefficients. In section 4 we give an example for the PAC scenario involving a copolymer which consists of blocks of HP-affine and nonaffine monomers.

We note the following relations for the bulk state ($\phi = 0$ and $c = c_b$):

$$\mu = \ln\left(\frac{c_b}{1-c_b}\right) - \chi(2c_b - 1) \qquad \text{and} \qquad \Pi = -\ln(1-c_b) - \chi c_b^2 \tag{2}$$

as well as the Gibbs–Duhem relation: $\Pi = \mu c_b - f_b(c_b)$, where f_b denotes the free energy per unit volume of the bulk. The symmetry of the bulk solution is broken by μ only, thus the coexistence line is defined by $\mu = 0$ and given by

$$\chi_x(c_b) = \frac{\ln\left(\frac{c_b}{1-c_b}\right)}{2c_b - 1} \tag{3}$$

This is sketched in Figure 1 on the lhs with the blue line. The critical point is given by $c_c = 1/2$ and $\chi_c = 2$. We introduce the parameter

$$\eta = \chi - \chi_c = \chi - 2 \tag{4}$$

which is taken as positive in the following. A completely dissolved bulk state of HP is given by $\mu < 0$ for $\eta > 0$ which is sketched by the blue line on the rhs of Figure 1.

We now turn to the free energy inside the polymer volume. With respect to the symmetry of the bulk phase at $c = 1/2$ we introduce the variable δ as

$$c = \frac{1}{2}(\delta + 1) \tag{5}$$

In the spirit of the Landau-model we expand the free energy in eq 1 with respect to δ and ϕ and we sort the terms in the order of the powers of δ as follows:

$$f_v(\delta|\phi) = f_0 + f_h + f_1 + f_{ev} + f_{el} + \Pi \tag{6}$$

with

$$f_0 = -\frac{1}{4}(\eta - 2\phi)\delta^2 + \frac{1}{12}\delta^4 \tag{7}$$

$$f_h = -\frac{1}{2}\mu\delta - \frac{1}{2}(\eta + \epsilon)\phi\delta + \frac{1}{3}\phi\delta^3 \tag{8}$$

$$f_1 = -\frac{1}{2}\mu - \frac{1}{2}\phi(\eta + \epsilon + 4 - \ln 4) \tag{9}$$

$$f_{ev} = \frac{1}{1-\delta}\phi^2 + \frac{2}{3}\frac{1}{(1-\delta)^2}\phi^3 \tag{10}$$

The symmetric contribution f_0 represents the nontrivial bulk free energy at phase coexistence, that is, in the absence of the field (chemical potential).

We can read-off some interesting physics from the Landau-type expansion. First, without the symmetry-breaking contribution, f_h, we obtain the phase-coexistence located at $\pm\,\delta_0$ with

$$\delta_0^2 = \frac{3}{2}\eta \tag{11}$$

This corresponds to the volume fractions of the diluted (−) and the condensed (+) phases of the bulk at phase coexistence.

The symmetry breaking field is given by $f_h = -h\delta$ with

$$h = \frac{1}{2}(\epsilon\phi + \mu) \tag{12}$$

Here, we have used the approximation $\delta^3 \simeq \delta\delta_0^2$ in f_h. The bulk behavior is given by $\phi = 0$, and $\mu < 0$. Thus, for the bulk state we have $h < 0$ and the lower minimum close to $-\,\delta_0$ is dominating, see blue line on the rhs of Figure 1. With increasing polymer concentration, the condensed phase becomes the stable one for $\phi > \mu/\epsilon$. One can regard the polymer field, $\epsilon\phi$, as shifting the effective chemical potential of the bulk to a virtual concentration $c_b' \simeq c + \gamma(\eta + \epsilon)\phi$ which is located in the coexistence region, as indicated by the red open circle on the lhs of Figure 1. Here, γ denotes a strictly positive prefactor. We note that the polymer field shifts the critical point too, see eq 7. However, this effect would be only of interest if $\phi \simeq \eta/2$. In the following we will consider the case $\phi \ll \eta$ and disregard this shift.

https://doi.org/10.1021/acs.macromol.2c00244
Macromolecules 2022, 55, 4841−4851

The terms in f_1 correspond to δ-independent contributions. The absolute contribution of the chemical potential due to the shift from the c- to the δ-variable can be disregarded. The second negative term in f_1 corresponds to the reduction of the mean-field interaction for $\delta = 0$. We note that the contribution 4−ln 4 is due to the additional mixing entropy of HP in the binary water−polymer environment. The excluded volume contribution corresponds to the usual expression in the reduced volume for the polymer in the presence of HP, that is, $\phi' = \phi/(1 - c)$.

In order to find the equilibrium state of the polymer-phase with respect to the bulk phase, first we obtain the global minimum of $f_v(\delta|\phi)$ for a given value of ϕ, which we denote as $f_v(\phi)$. In the following we will ignore f_{el}, since we focus on the condensed state where the chain is compressed and not stretched. Further below we discuss the validity of this approximation. The zero-order approach is to the consider the location of the two minima for $h = 0$, given by δ_0, see eq 11. Then, the leading order contribution to $f_v(\phi)$ is given by

$$f_v(\phi) \simeq -\frac{1}{2}\epsilon\phi\delta_0 - \frac{1}{2}\phi(\epsilon + \eta + 2s) - \mu\delta_0 + \frac{1}{1 - \delta_0}\phi^2 \tag{13}$$

where we have introduced the entropic contribution to the polymer field by $s = 2-\ln 2$. We note that we consider $\mu < 0$ and thus the bulk contribution has to be taken at $\delta_b = -\delta_0$, leading to an additional term $-\frac{1}{2}\mu\delta_0$. The osmotic pressure, Π, see eqs 1 and 6, corresponds to the negative free energy per volume unit of the bulk at given chemical potential. In eq 13 we have, therefore, subtracted all terms in eqs 7−9 with $\phi = 0$ and $\delta_b = -\delta_0$ which corresponds to $f_b(\mu)$, and thus $-\Pi$, in the Landau approximation. Thus, $f_v(\phi)$ is nothing but the difference between the polymer free energy and the bulk free energy. Furthermore, we have restricted the excluded volume interaction to the second virial coefficient. We note that at this level we can also take into account the Des Cloizeaux result $f_{ev} = a\phi^{9/4}$ with a numerical constant a instead.[33]

In order to find the equilibrium polymer volume fraction, ϕ, we have to consider the total free energy difference of the droplet with respect to the free energy of the bulk in the same volume as the droplet. Since the polymer volume is given by $V = N/\phi$ and thus a function of ϕ, the free energy per monomer, that is, $f(\phi) = f_v(\phi)/\phi$ has to be minimized instead. The minimum of the free energy per monomer, $f(\phi)$, is located at

$$\phi_0^2 = |\mu|\delta_0(1 - \delta_0) \tag{14}$$

We note that the first two terms in eq 13 are proportional to ϕ, so they become constant in $f(\phi)$ which is why the location of the minimum does not depend on ϵ. We can check the validity of the assumption $\phi \ll \eta$ made above, which reads: $|\mu| \ll \eta^{3/2}$. Thus, for states of the HP bulk far away from the coexistence point (larger values of $|\mu|$) the shift of the critical point due to the polymer field has to be considered.

The essential physics for the collapsed state of the polymer is given by the interplay between the free energy gain due formation of the condensate, third term in eq 13, and the excluded volume repulsion according to the last term in eq 13. Written in terms of the radius of gyration of the polymer, R, instead of the monomer density, ϕ, the corresponding free energy of the whole polymer reads:

$$F = R^3 f_v(\phi) = |\mu|\delta_0 R^3 + \frac{1}{1 - \delta_0}N^2/R^3 \tag{15}$$

where constant terms and prefactors of order unity are dropped. The equilibrium value is given by the scaling relation $R^3 \sim N|\mu|^{-1/2}$ and thus $F_{min} \sim N|\mu|^{1/2}$. The elastic contribution to the free energy would contribute as $R^2/N \sim N^{-1/3}|\mu|^{-1/3}$. Thus, our solution is limited to an absolute value of the chemical potential larger than $|\mu^*| \sim N^{-8/5}$ (not too close to the bulk coexistence) which, however, is a very small number for large polymers with $N = O(1000)$. However, this corresponds to a lower limit of the monomer concentration given by the overlap value, that is: $\phi_0 > \phi^* \sim N^{-4/5}$. We note that values of $\mu < \mu^*$ give rise to a more subtle physics where the elasticity of the polymer limits the stability of the PAC droplet which is taken into account in the full numerical solution. However, we note that this limiting case is difficult to prepare and will be very sensitive with respect to small changes in bulk concentration of HP, and thus will be of less interest in biology or in ternary solutions of polymers.

In the inset of Figure 2 we display the numerical result for the monomer concentration as a function of the absolute value

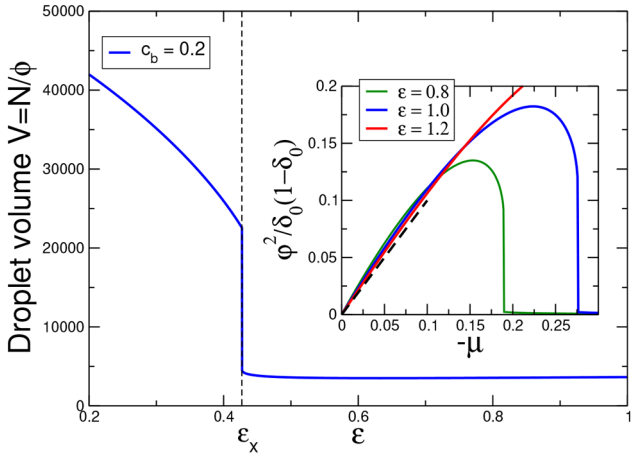

Figure 2. Volume of PAC-droplet vs strength of the HP-polymer interaction. The HP solution is set to $\chi = 2.2$ ($\eta = 0.2$) and $c_b = 0.2$ well below the bulk condensation point at $c_x \simeq 0.25$ according to eq 3. The degree of polymerization used in the numerical solution is $N = 500$. In the condensed state ($\epsilon > \epsilon_x \simeq 0.427$) the droplet volume is nearly independent of ϵ. Inset: Rescaled squared monomer concentration vs absolute value of the chemical potential of the HP solution for $\epsilon = 0.8$, 1, 1.2. As predicted in the approximate solution, eq 14, dashed line, the polymer concentration rises with decreasing HP concentration (increasing absolute value of the chemical potential) and is nearly independent of the interaction with the polymer.

of the chemical potential of the HP-solution for selected parameters of ϵ and for $\chi = 2.2$. All numerical results are obtained by finding the global minimum of the free energy per monomer unit derived from eq 1, that is, for $f(c|\phi) = f_v(c|\phi)/\phi$ and with a degree of polymerization $N = 500$. A nearly linear behavior between the square of the equilibrium monomer concentration and the chemical potential can be observed for smaller values of $-\mu$.

According to eq 14 the volume of the condensate droplet, $V_d \sim 1/\phi_0 \sim |\mu|^{-1/2}$, shrinks with decreasing HP-concentration in the bulk. That means, that very close to the bulk coexistence, $|\mu| = 0$, droplets of maximum size are formed which decrease in size up to the transition, estimated by eq 16. While this seems intuitive (smaller droplets for smaller HP-concentration), it

https://doi.org/10.1021/acs.macromol.2c00244
Macromolecules 2022, 55, 4841−4851

means that at the transition (minimum HP volume fraction in the bulk) the maximum degree of collapse of the polymer is observed and that the polymer-droplet expands once again upon adding more HP to the solution.

Given the optimal value of the polymer concentration we localize the transition to the condensed state by using eq 12 and $h(\phi_0) = 0$:

$$\epsilon_x = \left[\frac{|\mu_x|}{\delta_0(1-\delta_0)}\right]^{1/2} \sim |\mu_x|^{1/2} \tag{16}$$

where the index "x" indicates the transition between the formation and dissolution of polymer assisted condensates.

A second conclusion taken from eq 14 regards the ϵ-dependence of the droplet size, which is absent in this approximation. Indeed the variation of the droplet-size with respect to the HP-polymer-selectivity is rather small as displayed in Figure 2 (behavior right of the transition point at $\epsilon_x \simeq 0.427$). This result is interesting since it shows the robustness of the droplet properties with respect to the interaction between HP and polymer: above a minimal value, ϵ_x, which marks the condensation transition, the droplet size only varies weakly with stronger interaction. We note that the fraction of methylated nucleosomes is reduced by a factor of 2 after replication, which should still be sufficient to form the heterochromatin state, which in turn can recruit fresh methylase into the HP-rich droplets and thus the average interaction is increased to the original level. In our model such strong fluctuations in HP-polymer-interaction would not have much impact on the properties of the PAC condensate.

In the upper part of Figure 3 we display the relative HP-concentration in the polymer volume for various values of the HP-polymer interaction as obtained from the numerical solution. As expected, below the PAC transition, the ratio is very close to unity since the weak HP-polymer interaction cannot bind any substantial amount of HP without the collective effect of HP. This is followed by a jump-like increase above the transition point. The excess of the HP in the condensate is of the order 2−3 for the parameters chosen here. We note that due to the polymer collapse the total volume fraction of the condensate (HP + polymer) is typically of the order 0.6−0.8.

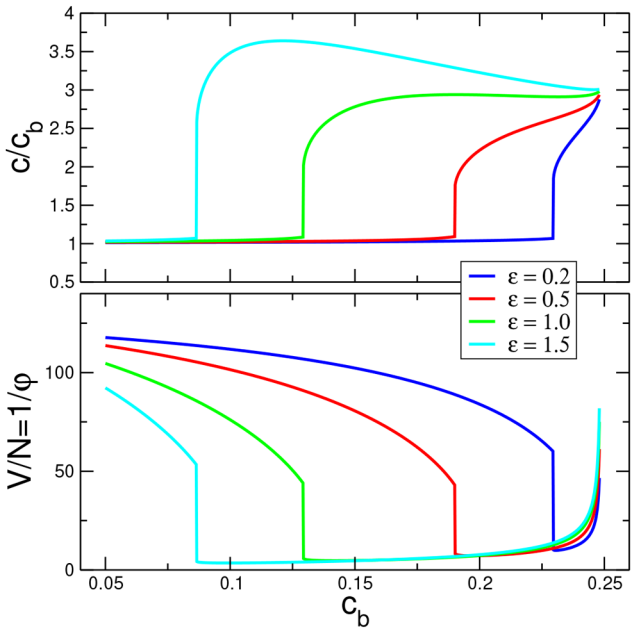

Figure 3. Upper panel: relative HP volume fraction in the polymer volume vs bulk volume fraction, c_b. Lower panel: Droplet volume per monomer unit vs c_b. The HP solution is set to $\chi = 2.2$ and the bulk condensation point is located at $c_x \simeq 0.25$.

The volume of the polymer coil in monomer units vs the HP concentration in bulk is displayed in the lower panel of Figure 3. Increasing the HP concentration to the coexistence condition, see approximate solution in eq 16, leads to a jump-like contraction of the polymer along with the formation of the HP-polymer-condensate. Further increase of the amount of HP in the bulk leads to a smooth increase of the droplet volume which is associated with an increase of the HP-fraction.

On the lhs of Figure 4 we show the phase diagram as predicted by eq 16. The surface corresponds to the function $\epsilon_X(c_b, \chi)$. The PAC scenario is bounded by the bulk phase transition for larger values of c_b and χ respectively, see eq 3, as indicated by the blue line. The rhs of Figure 4 displays a comparison between the numerical solution of the full free energy model (data points) and the Landau-type approximation (yellow line) for the case $\chi = 2.2$. We note that the numerical solution can be easily extended to the case of larger size ratio of HP to water by considering $n > 1$ in eq 1.

Although our results have been derived under the assumption of a single polymer forming the condensate, they can be directly extended to many chains. For long chains, $N \gg 1$, the translational entropy inside a common droplet is irrelevant. Thus, all arguments in our theory presented above remain valid and the polymer volume fraction, ϕ, is understood as the volume fraction of all chains forming the PAC condensate. The concentration, ϕ_0, necessary to induce PAC, see eq 14, corresponds to a semidilute state of the polymers inside the droplet. The equilibrium size of the droplet will then be controlled by the number of polymers available in the system. An interesting question arises whether a multichain droplet, or a macroscopic phase separated state, is thermodynamically favored with respect to single-chain PAC-condensates (S-PAC's). On the level of S-PAC's, the system resembles a particle gas and the transition to the macroscopic condensed state is driven by the effective interactions between S-PAC's. When an S-PAC joins the macroscopic PAC-phase, two effects have to be considered: the surface tension and the possible change in the conformation entropy of the chains. Since the polymer chains gain only a small amount of conformation entropy by joining in a larger droplet at the same concentration, the latter contribution could be practically neglected. However, the surface tension of an S-PAC is low since HP-HP interactions are weaker than necessary to form a phase segregated state in the bulk. This is in contrast to the case of chains in poor solvent where the gain in free energy by transferring an individual chain from the isolated collapsed state in poor solvent into the condensed bulk is of the order of $N^{2/3}$, see ref 34 for a recent study, while for PAC the prefactor is expected to be much lower because of the above-mentioned low surface tension of S-PAC's. Therefore, the concentration regime where S-PAC's dominate should be much larger as for chains in poor solvent. However, the expected low surface tension of PAC-condensates reduces the effect of the Laplace-pressure, which we did not take into account here. In case of heterochromatin, where the typical radii are of the order of micrometer, this might therefore be small.

https://doi.org/10.1021/acs.macromol.2c00244
Macromolecules 2022, 55, 4841−4851

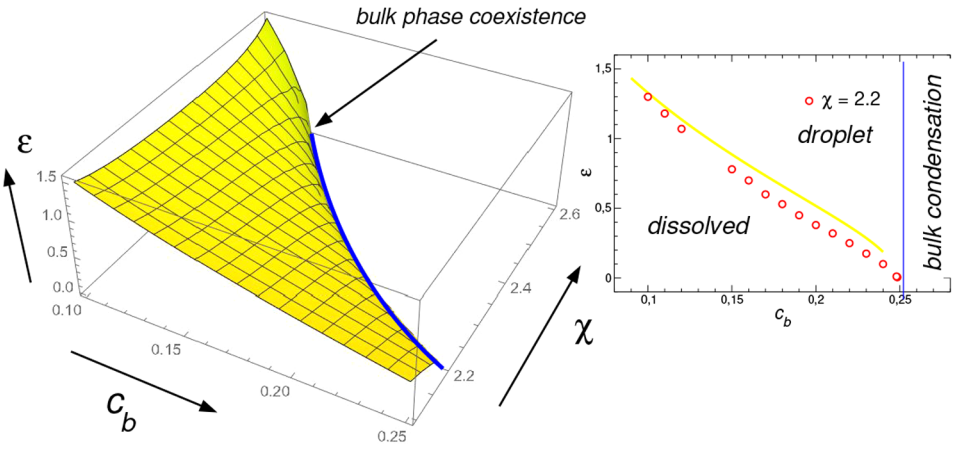

Figure 4. Left: Phase diagram as predicted by eq 16. The blue line marks the bulk phase transition in the (c_b, χ)-plane. States above the surface are polymer-assisted condensates. Right: Phase coexistence obtained from the numerical solution for $\chi = 2.2$ (○) compared with the analytical approximation from eq 16. The vertical blue line indicates the bulk phase transition.

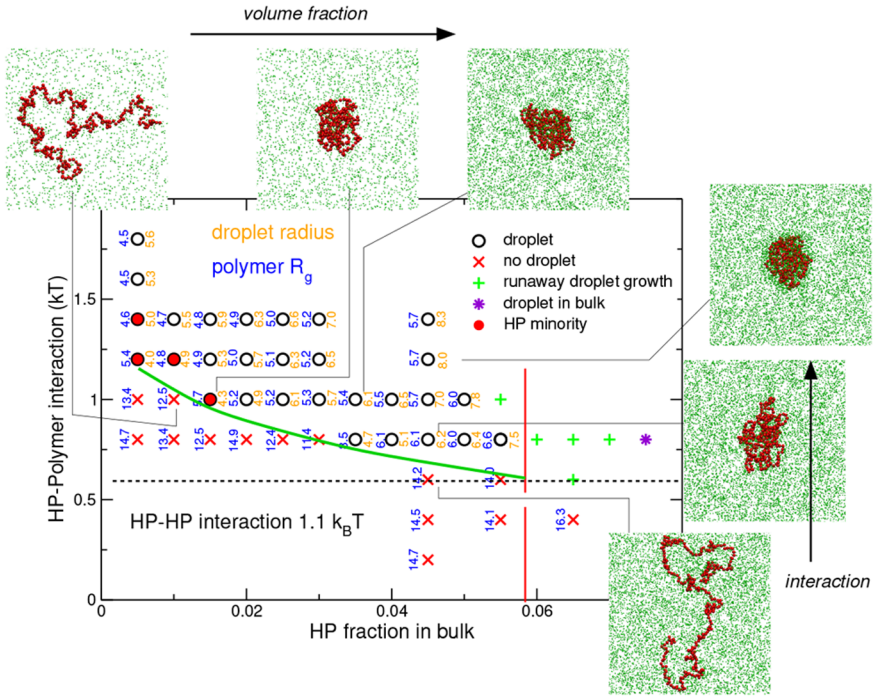

Figure 5. Phase diagram of the simulated system for a polymer chain of length $N = 300$. The LJ-interaction parameter among HP-beads is chosen as $\chi_S = 1.1$, well above the critical point. The bulk condensation transition is indicated by the red vertical line. The green line sketches the phase boundary between the droplet and the dissolved state, as predicted in Figure 4. The dashed horizontal line indicates the threshold to HP-polymer adsorption, that is, $\epsilon = 0$ in the mean-field model. Circles indicate droplet states while crosses symbolize dissolved states. Points to the right of the red line belong to bulk condensed states. Snapshots from the simulations are displayed for selected parameters. The numbers on both sides of the data points denote the radius of gyration of the polymer (blue) and the droplet-radius (orange), respectively. The latter is defined as the distance from the droplet center at which the density drops to half of its center value.

Another generalization of the present model is to take into account the effect of a thermal solvent for the polymer in aqueous solution. There are several studies indicating that chromatin displays features which correspond even to poor solvent behavior.[35−41] As a result, the volume ratio between the polymer in the absence of PAC and the PAC-condensate should be smaller as predicted for the athermal case, see Figure 2. On the level of our mean-field model, thermal solvent conditions can be incorporated by adding the standard Flory−Huggins-type interaction contribution in the form of $f_T = \chi_P\phi(1 - \phi - c)$ to the free energy given in eq 1, where χ_p denotes the interaction between polymer and common solvent (water). The consequence of this contribution is a shift in the effective HP-polymer interaction according to $\epsilon \to \epsilon + \chi_p$, and an increase in the equilibrium polymer density according to the reduced effective excluded volume interaction according to $\phi_0^2 \to \phi_0^2/(1 - \chi_p(1 - \delta_0))$, where the last expression refers to the result in eq 14. In essence, the consideration of thermal solvent conditions for the polymer will reduce the predicted density ratio of heterochromatin and euchromatin, that is, between the PAC-condensate and the polymer in the absence

https://doi.org/10.1021/acs.macromol.2c00244
Macromolecules 2022, 55, 4841−4851

of HP. The case of $\chi_p > 1/2$, that is, poor solvent conditions for the polymer in the absence of HP deserves further consideration. In this case the second virial coefficient in eq 10 can become negative and the equilibrium polymer density, ϕ_0, is determined by the third viral coefficient.

3. MOLECULAR DYNAMICS SIMULATIONS

To test the predictions of our mean-field theory, we have carried out molecular dynamics simulations using a standard bead−spring model for the polymer chain, and representing HP molecules by unconnected beads (of the same diameter as the monomers) in the background of an implicit solvent model. Pair interactions are Lennard-Jones (LJ) potentials

$$U_{\mathrm{LJ}}(r) = 4\epsilon_{\mathrm{LJ}}\left[\left(\frac{b}{r}\right)^{12} - \left(\frac{b}{r}\right)^{6} - \left(\frac{b}{r_c}\right)^{12} + \left(\frac{b}{r_c}\right)^{6}\right] \quad (17)$$

where $b = 1$ stands for the bead diameter (and unit-length), ϵ_{LJ} for the interaction strength and r_c for the cutoff distance. Interactions between monomers are truncated at $r_c = 2^{1/6}$, the minimum of the LJ-potential, thus repulsive and simulating polymers inside a good implicit solvent. The attractive interactions between HP-beads use $\epsilon_{\mathrm{LJ}} \equiv \chi_S = 1.1$ and a cutoff distance of $r_c = 2.5$, whereas HP-monomer interactions apply varying strengths $\epsilon_{\mathrm{LJ}} \equiv \epsilon_S$ and are truncated at $r_c = 2.5$. Here, the index "S" indicates the values used in the simulation model. First, we note that due to the hard-core repulsion, a minimum value of ϵ_S is necessary to realize a crossover from repulsion to adsorption of the HP-beads with respect to the polymer chain. This has been studied with the same simulation model in a previous work,[42] see Figure 4 therein, and is given by $\epsilon_{S0} \simeq 0.6$. The bulk phase diagram of the LJ-system has been studied before[43] and the critical point was found to be located at $\chi_X \simeq 0.9$ and $c_X = 0.32$. Our choice of $\chi_S = 1.1$ is thus located well above the critical point. The transition to the condensed phase is located at about $c_b \simeq 0.0575$, while the chain length in our simulations is $N = 300$. Simulations are carried out using the LAMMPS molecular dynamics package.[44]

The main results from our simulations are displayed in the phase diagram in Figure 5. We observe PAC at HP-concentrations well below the bulk phase coexistence, to the left of the vertical red line, as indicated by the open circles. In these states droplets are formed in equilibrium with the surrounding bulk which are restricted in size by the polymer. PAC is bounded by a concentration-dependent HP-polymer interaction, $\epsilon_X(c_b)$, which is sketched by the green line in the phase diagram. As compared to the symmetric FH-model the condensation is shifted to lower values of the HP concentration. This is a consequence of the asymmetry of the LJ-system (spheres vs implicit solvent). Otherwise, we can recognize all features as predicted from the mean-field model, see Figure 4. The snapshots display a sharp boundary between the droplet and the bulk phase, and droplets are usually dominated by highly elevated concentrations of HP-molecules. An exception occurs at very low HP-bulk-concentrations at which, close to the phase boundary, the collapsed polymer phase contains only a minority of HP-molecules (red dots in the phase diagram). Here, HP plays the role of a gluonic solvent which forms temporary bridges between monomers as described in ref 45. We note that such a state of the HP-polymer-condensate corresponds to the one assumed in a recent work by Spakowitz and co-workers.[46]

The droplet radius may either be defined from its radial density distribution, orange colored numbers in Figure 5, or—since they are so closely related—from the size of the collapsed polymer itself, blue colored numbers. In Figure 6 we display

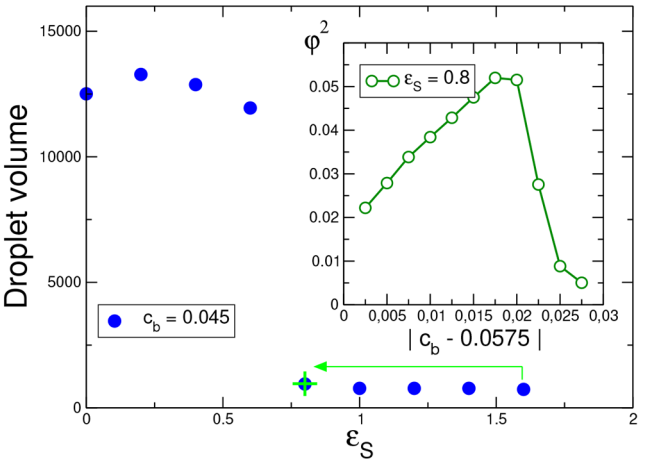

Figure 6. Volume of polymer droplet vs strength of the HP-polymer interaction in simulation units. The HP bulk solution is set to $c_b = 0.045$, well below the bulk condensation point at $c_x \simeq 0.0575$. The degree of polymerization is $N = 300$. In the condensed state ($\epsilon > \epsilon_x \simeq 0.7$) the droplet volume is nearly independent of ϵ_S. Inset: Squared monomer concentration vs distance to the condensation point, $|c_b - c_x|$ of the HP solution for $\epsilon_S = 0.8$. The green cross indicates the result for $\epsilon_S = 1.6$ where only half of the monomers were randomly chosen to be attractive for HP.

the droplet volume as defined by $V = 4\pi R_g^3/3$, where R_g denotes the radius of gyration of the polymer chain. By crossing over the transition point at about $\epsilon_X \simeq 0.7$, the polymer collapses and the droplet volume turns nearly independent of the HP-polymer interaction as predicted by the mean-field model.

Following the result of the analytical section, see in particular eq 14 and the inset in Figure 2, we have calculated the squared monomer density vs the distance of the bulk concentration to the coexistence point, $\Delta c = |c_b - c_x|$. Here, we have taken the plateau of the monomer concentration profile to calculate c. Since we do not have an analytic expression for the chemical potential of the LJ-fluid, we make use of the fact that close to the coexistence point, the chemical potential varies linearly with Δc, that is, $\mu = \mu_X - a\Delta c$ with some constant a, and μ_X denoting the chemical potential at coexistence (which is zero for the symmetric FH-model). The result is displayed in the inset of Figure 6 and can be compared to the prediction of the theory as shown in the inset of Figure 2. As predicted, the polymer exhibits its maximally collapsed state at the transition point at the lowest HP volume fraction (larger values of Δc), and then expands when the amount of HP is increased up to the bulk coexistence point ($\Delta c \to 0$).

In addition to these results we have performed simulations in which the attractive energy of $\epsilon_S = 1.6$ applies only for a randomly chosen fraction of the monomers, while the other monomers have no preferential interaction with HP, that is, $\epsilon_S = 0$. This corresponds to the case of heterochromatin just after cell division where half of the methyl-groups are missing in each daughter cell. The green cross in Figure 6 corresponds to

https://doi.org/10.1021/acs.macromol.2c00244
Macromolecules 2022, 55, 4841−4851

the simulation with a fraction of 1/2 of attractive monomers only. We obtain almost the same value for the droplet volume as for the reduced interaction $\epsilon_S/2$ in the homogeneously labeled chain (the difference being of the order of 1% here).

In Figure 7 we display the radial density profile of HP as a function of the distance to the center of mass of the polymer

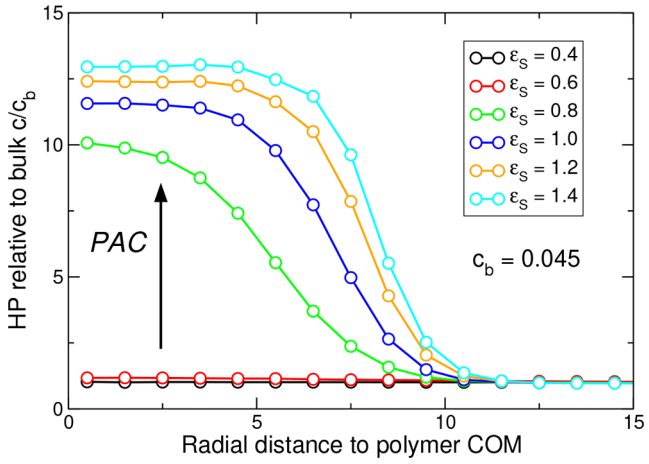

Figure 7. Rescaled radial density profile of HP concentration taken from the center of mass (COM) of the polymer for various values of the HP-polymer interaction constant at the bulk density c_b = 0.045. The PAC transition (arrow) occurs in between ϵ_S = 0.6···0.7.

normalized by the bulk density for c_b = 0.045, and for various values of ϵ_S. The PAC transition occurs in the interval between ϵ_S = 0.6···0.7 (compare with Figure 5). The jump in the HP density between bulk and droplet state is up to a factor of 12.

To conclude this section, we have shown that PAC of a binary fluid can be observed in molecular dynamics simulations. Although a direct quantitative comparison is not easily possible due of the difference between the equations of state for the LJ-model and the FH-model, all the features predicted by the simple analytical model are displayed semiquantitatively in the simulated system, including the phase diagram. In particular, the robustness of the properties of the HP-polymer droplets with respect to the HP-polymer interaction is also shown in the simulated model.

4. DISCUSSION AND CONCLUSIONS

What is most remarkable about the presented model of PAC is the fact that a discontinuous phase transition is induced in a small system, the extension of which is strictly limited by the presence of the polymer. In fact, the HP-polymer droplet cannot nucleate a macroscopic phase transition in the bulk, since the condensed phase is stable only in the presence of a polymer. Our model can be extended to copolymers where individual sequences are tagged as HP-affine ($\epsilon > 0$) while the other monomers behave neutral or repulsive with respect to HP. An example is shown in Figure 8 for the case of a 9-block copolymer. The only difference is the free energy effort of loop formation, which is of order $k_BT \ln N_b$ per loop, where N_b denotes the number of monomers per HP-repulsive block. The core of the unimolecular micelle is formed by PAC and contains a major fraction of HP. This example also illustrates the formation of PAC by many chains (blocks). In addition to the points discussed at the end of section 2 concerning multichain condensates, the nontagged sequences (mimicking

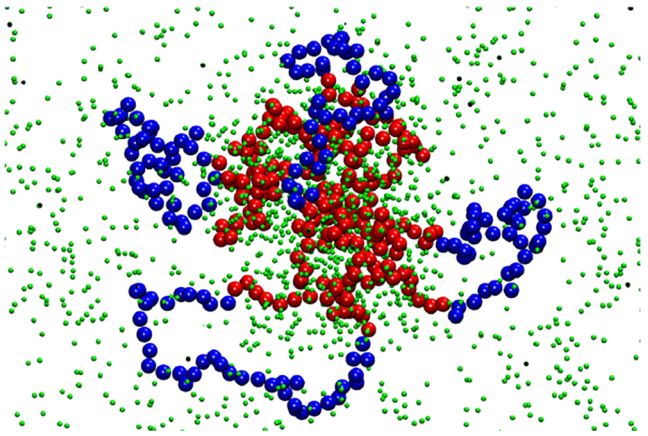

Figure 8. Snapshot of a block copolymer which is composed of 5 blocks of HP-affine monomers (ϵ_S = 1.0, colored red), and of 4 blocks of HP-repulsive monomers (ϵ_S = 0, colored blue) immersed in a solution with HP of volume fraction c_b = 0.045. Each block contains 40 monomers. The HP-affine blocks form the core of a unimolecular micelle driven by PAC. HP molecules are displayed in green. For a better visibility we decreased the size of HP molecules in the snapshot.

euchromatin) provide a surfactant-like effect: Increasing the number of blocks in the PAC-micelle increases the free energy effort to eventually form a brush-like state of the loops and thus limits the size of the condensate. As a consequence two scenarios are possible in equilibrium: First, multiple micelles are formed in a single very large polymer (that is, several heterochromatin domains in the same chromosome). Second, tagged blocks from different polymers can join into the same core (that is, heterochromatin domains can be shared by chromosomes). Which of the scenarios is realized depends on the length of sequences and their number in the same polymer.

Let us note the similarity of the result for the polymer coil size with respect to the HP concentration, lower part of Figure 3, with the well-known cononsolvency effect observed in some polymers.[45,47−50] Cosolvents, frequently low alcohols such as methanol and ethanol, when admixed to water can cause a collapse of polymers such as poly(*N*-isopropylacrylamide) (PNiPAAm) in an intermediate concentration region with a similar re-entrance behavior of the polymer volume as shown in Figure 3. The difference with respect to PAC is that the alcohol−water mixtures are fully miscible ($\chi \simeq 0$) and the polymer collapse is a result of an effective monomer−monomer-attraction induced by the nonspecific preferential attraction of the cosolvent by the polymer, which can be associated with the formation of temporary cosolvent-bridges between monomers.[49,50] This mechanism has been termed as "gluonic" in a previous work.[45] In this case the gluonic solvent (cosolvent) is essentially bound to the monomers and higher values of ϵ, significantly above $1k_BT$, are necessary.[42] In the case of PAC already weak preferential interactions below $1k_BT$ between HP and the polymer can trigger a stable droplet formation. The computer simulations presented in this work give indications for the gluonic regime in the case of very low HP-concentration and high protein−polymer interactions, see Figure 5.

A particularly interesting aspect of PAC is that HP forms the major fraction in the droplet volume which therefore leads to its fluid-like property,[51] while the gluonic mechanism leads to a gel-like polymer scaffold which hosts a smaller fraction of the

https://doi.org/10.1021/acs.macromol.2c00244
Macromolecules 2022, 55, 4841−4851

rather strongly bound protein. This is related with a well-defined fluid phase boundary of the PAC droplet only. Therefore, the PAC droplet can form a reaction container for other molecules and enzymes which are soluble and attracted to the protein-enriched liquid phase. Another difference concerns the robustness of the droplet with respect to drastic changes in the polymer−protein interaction, which we have denoted here as ϵ. Only low values of $\epsilon < k_BT$ are necessary for PAC but also larger values result in a liquid phase in PAC since the dense phase of protein around the polymer merely leads to a saturation of adsorption and not to strong coupling effects between the monomers. In our simulations we have also considered the case where only half of the monomers (randomly selected) are attractive with respect to HP. The results are analogous to the case of reducing the HP-monomer attraction. This indicates the stability of PAC with respect to addition/dilution of methylated nucleosomes for the case of heterochromatin.

By contrast the gluonic binding and bridging scenario leads to strongly immobilized proteins which form transient bonds between the monomers of the polymer host. In this context it is interesting to discuss the model by Spakowitz and co-workers for epigenetic inheritance.[46] This model was originally developed to calculate the contact map of an entire human genome.[52] Such contact maps are now routinely measured by chromosome conformation capture techniques.[14] An experimentally determined methylation profile served as input for a coarse-grained chromatin model with nucleosome resolution.[46,52] The model explicitly takes into account the (coarse-grained) HP1 molecules, which bind preferentially to methylated nucleosomes and then form bridges to other bound HP1s nearby. The Monte Carlo (MC) simulations have indeed successfully reproduced an experimental contact map.[52] In the later study[46] this model was then used to investigate the inheritance of epigenetic tags through mitosis. An MC simulation was performed to determine 26 equilibrium polymer configurations and HP1 binding profiles, which were used as an input to calculate steady state methylation probabilities. For the latter, it was assumed that the on-rate of methylation for a nucleosome is proportional to the number of HP1-bound tails near that nucleosomes (while the off-rate is not). Each cycle was considered to be one cell generation. It was shown that the methylation profiles could be inherited stably over various cell generations. To achieve this, however, the HP1 concentration had to be carefully adjusted to the given reaction rates. If the HP1 concentration was changed only slightly to larger or smaller values, the proportion of methylated nucleosomes would either increase or decrease with each subsequent cell generation (see Figure 2 in ref 46). It should be further noted that the chromosome conformations were frozen during the methylation reaction and were determined from the methylation state of the previous cycle, that is, before cell division, instead of being sampled afresh beginning with a semimethylated state. This could affect both the conformations and the resulting methylation profiles.

This suggests to us that this scenario does not give the full picture. On the one hand, it shows strong bridging interactions between nucleosomes, which would rather lead to a gel-like state (gluonic scenario) that could hinder the free diffusion of, for example, the methylases through the heterochromatic region. On the other hand, a mechanism would be needed that ensures that the right concentration of HP1 molecules is always present to avoid a runaway mechanism. In contrast, the PAC scenario offers liquid-like heterochromatin compartments that are robust against changes in system parameters such as the concentration of HP1 proteins. At this point it remains to be seen whether the PAC system with a block polymer alone is sufficient for the reliable inheritance of heterochromatin or whether additional components (for example, insulators as described in the introduction) need to be present to prohibit an increasing number of euchromatic nucleosomes getting sucked into the droplets over time to become enzymatically tagged as heterochromatic. We plan to address these questions in a future study.

The motivation of our work was focused upon HP1 as an example for a droplet-forming protein. This protein has a direct binding site for H3K9me3 marks. Nucleosomes with this tag are part of what is known as constitutive heterochromatin, a type of heterochromatin that in all cell types includes regions near the telomeres and around the centromeres of the chromosomes. However, the modification H3K27me3 marks facultative heterochromatin (heterochromatin that is compact only in a subset of cell types). In this case, the role of HP1 could be played by the Polycomb Repressive Complex 1 (PRC1), a protein complex known to have the ability to form condensates and to have specific attraction to H3K27me3 marks.[53] Remarkably, the droplets contain their own enzyme that places another, shorter-lived marker on the corresponding nucleosomes, which presumably leads to only a subset of genes ending up in a condensed state for a given cell type.[53] Therefore, systems of droplets produced by PAC, which organize blocks of nucleosomes into sets of loops, might serve as a platform for transmitting epigenetic memory across cell generations. Finally, we note that similar mechanisms might be at work at many places in the cell, in the context of chromatin but also for many biomolecular condensates that are not in contact with DNA. In the latter case, RNA molecules could play the role of the polymer that assists the condensation.[22]

Besides the biological examples which have motivated our study, PAC can also be expected for synthetic polymer/solvent/cosolvent mixtures. An interesting example here is a mixture of water and 1-butanol. At room temperature this system is miscible up to a volume fraction of about 10% of 1-butanol[54] only. In such a mixture PNiPAAm can play the role of the weakly selective polymer, here with respect to 1-butanol, which can induce condensation of 1-butanol. The marked difference to the gluonic effect as described above is again that the cosolvent does not have to form bridges between the monomers, but that the polymer is totally engulfed by the alcohol.

To conclude, the scenario of polymer-assisted condensation is a new type of transition in three-component polymer−solvent systems and stands well aside from the scenario of preferential adsorption/binding and bridging of cosolvents/cosolutes. For PAC it requires only a weak attraction to tip-over the binary solution into the cosolvent-rich condensed state, which, at the same time, is restricted by the presence of the polymer.

AUTHOR INFORMATION

Corresponding Author

Jens-Uwe Sommer − *Leibniz-Institut für Polymerforschung Dresden, 01069 Dresden, Germany; Cluster of Excellence Physics of Life, TU Dresden, 01307 Dresden, Germany;* orcid.org/0000-0001-8239-3570; Email: sommer@ipfdd.de

https://doi.org/10.1021/acs.macromol.2c00244
Macromolecules 2022, 55, 4841−4851

Authors

Holger Merlitz − *Leibniz-Institut für Polymerforschung Dresden, 01069 Dresden, Germany*

Helmut Schiessel − *Cluster of Excellence Physics of Life, TU Dresden, 01307 Dresden, Germany; Institut für Theoretische Physik, Technische Universität Dresden, 01062 Dresden, Germany*

Complete contact information is available at: https://pubs.acs.org/10.1021/acs.macromol.2c00244

Notes

The authors declare no competing financial interest.

■ ACKNOWLEDGMENTS

J.U.S. acknowledges support from the DFG under the grant number SO-277/17. H.S. and J.U.S. were supported by the Deutsche Forschungsgemeinschaft (DFG, German Research Foundation) under Germany's Excellence Strategy−EXC2068−390729961−Cluster of Excellence Physics of Life of TU Dresden.

■ REFERENCES

(1) Goloborodko, A.; Imakaev, M. V.; Marko, J. F.; Mirny, L. Compaction and segregation of sister chromatids via active loop extrusion. *eLife* **2016**, *5*, No. e14864.

(2) Gibcus, J. H.; Samejima, K.; Goloborodko, A.; Samejima, I.; Naumova, N.; Nuebler, J.; Kanemaki, M. T.; Xie, L.; Paulson, J. R.; Earnshaw, W. C.; Mirny, L. A.; Dekker, J. A pathway for mitotic chromosome formation. *Science* **2018**, *359*, No. eaao6135.

(3) Sanborn, A. L.; et al. Chromatin extrusion explains key features of loop and domain formation in wild-type and engineered genomes. *Proc. Natl. Acad. Sci. U.S.A.* **2015**, *112*, E6456−E6465.

(4) Fudenberg, G.; Imakaev, M.; Lu, C.; Goloborodko, A.; Abdennur, N.; Mirny, L. A. Formation of Chromosomal Domains by Loop Extrusion. *Cell Reports* **2016**, *15*, 2038−2049.

(5) Halverson, J. D.; Lee, W. B.; Grest, G. S.; Grosberg, A. Y.; Kremer, K. Molecular dynamics simulation study of nonconcatenated ring polymers in a melt. I. Statics. *J. Chem. Phys.* **2011**, *134*, 204904.

(6) Lang, M.; Fischer, J.; Sommer, J.-U. Effect of Topology on the Conformations of Ring Polymers. *Macromolecules* **2012**, *45*, 7642−7648.

(7) Grosberg, A. Y. Annealed lattice animal model and Flory theory for the melt of non-concatenated rings: towards the physics of crumpling. *Soft Matter* **2014**, *10*, 560−565.

(8) Rosa, A.; Everaers, R. Ring Polymers in the Melt State: The Physics of Crumpling. *Phys. Rev. Lett.* **2014**, *112*, 118302.

(9) Ge, T.; Panyukov, S.; Rubinstein, M. Self-Similar Conformations and Dynamics in Entangled Melts and Solutions of Nonconcatenated Ring Polymers. *Macromolecules* **2016**, *49*, 708−722.

(10) Smrek, J.; Grosberg, A. Y. Minimal Surfaces on Unconcatenated Polymer Rings in Melt. *ACS Macro Lett.* **2016**, *5*, 750−754.

(11) Schram, R. D.; Rosa, A.; Everaers, R. Local loop opening in untangled ring polymer melts: a detailed "Feynman test" of models for the large scale structure. *Soft Matter* **2019**, *15*, 2418−2429.

(12) Ghobadpour, E.; Kolb, M.; Ejtehadi, M. R.; Everaers, R. Monte Carlo simulation of a lattice model for the dynamics of randomly branching double-folded ring polymers. *Phys. Rev. E* **2021**, *104*, 014501.

(13) Parisi, D.; Costanzo, S.; Jeong, Y.; Ahn, J.; Chang, T.; Vlassopoulos, D.; Halverson, J. D.; Kremer, K.; Ge, T.; Rubinstein, M.; Grest, G. S.; Srinin, W.; Grosberg, A. Y. Nonlinear Shear Rheology of Entangled Polymer Rings. *Macromolecules* **2021**, *54*, 2811−2827.

(14) Sazer, S.; Schiessel, H. The biology and polymer physics underlying large-scale chromosome organization. *Traffic* **2018**, *19*, 87−104.

(15) Cortini, R.; Barbi, M.; Caré, B. R.; Lavelle, C.; Lesne, A.; Mozziconacci, J.; Victor, J.-M. The physics of epigenetics. *Rev. Mod. Phys.* **2016**, *88*, 025002.

(16) Luger, K.; Mäder, A. W.; Richmond, R. K.; Sargent, D. F.; Richmond, T. J. Crystal structure of the nucleosome core particle at 2.8 *Å* resolution. *Nature* **1997**, *389*, 251−260.

(17) Eslami-Mossallam, B.; Schiessel, H.; van Noort, J. Nucleosome dynamics: Sequence matters. *Adv. Colloid Interface Sci.* **2016**, *232*, 101−113.

(18) Yu, C.; Gan, H.; Serra-Cardona, A.; Zhang, L.; Gan, S.; Sharma, S.; Johansson, E.; Chabes, A.; Xu, R.-M.; Zhang, Z. A mechanism for preventing asymmetric histone segregation onto replicating DNA strands. *Science* **2018**, *361*, 1386−1389.

(19) Barkess, G.; West, A. G. Chromatin insulator elements: establishing barriers to set heterochromatin boundaries. *Epigenomics* **2012**, *4*, 67−80.

(20) Rao, S. S.P.; Huntley, M. H.; Durand, N. C.; Stamenova, E. K.; Bochkov, I. D.; Robinson, J. T.; Sanborn, A. L.; Machol, I.; Omer, A. D.; Lander, E. S.; Aiden, E. L. A 3D Map of the Human Genome at Kilobase Resolution Reveals Principles of Chromatin Looping. *Cell* **2014**, *159*, 1665−1680.

(21) Gaszner, M.; Felsenfeld, G. Insulators: exploiting transcriptional and epigenetic mechanisms. *Nature Reviews* **2006**, *7*, 703−713.

(22) Banani, S. F.; Lee, H. O.; Hyman, A. A.; Rosen, M. K. Biomolecular condensates: organizers of cellular biochemistry. *Nat. Rev. Mol. Cell Biol.* **2017**, *18*, 285−298.

(23) Larson, A. G.; Elnatan, D.; Keenen, M. M.; Trnka, M. J.; Johnston, J. B.; Burlingame, A. L.; Agard, D. A.; Redding, S.; Narlikar, G. J. Liquid droplet formation by HP1α suggests a role for phase separation in heterochromatin. *Nature* **2017**, *547*, 236−240.

(24) Strom, A. R.; Emelyanov, A. V.; Mir, M.; Fyodorov, D. V.; Darzacq, X.; Karpen, G. H. Phase separation drives heterochromatin domain formation. *Nature* **2017**, *547*, 241−245.

(25) Bannister, A. J.; Zegerman, P.; Partridge, J. F.; Miska, E. A.; Thomas, J. O.; Allshire, R. C.; Kouzarides, T. Selective recognition of methylated lysine 9 on histone H3 by the HP1 chromo domain. *Nature* **2001**, *410*, 120−124.

(26) Lachner, M.; O'Carroll, D.; Rea, S.; Mechtler, K.; Jenuwein, T. Methylation of histone H3 lysine 9 creates a binding site for HP1 proteins. *Nature* **2001**, *410*, 116−120.

(27) Nakayama, J.-i.; Rice, J. C.; Strahl, B. D.; Allis, C. D.; Grewal, S. I. S. Role of histone H3 lysine 9 methylation in epigenetic control of heterochromatin assembly. *Science* **2001**, *292*, 110−113.

(28) Sommer, J.-U.; Daoud, M. Adsorption of multiblock copolymers at interfaces. *Phys. Rev. E* **1996**, *53*, 905−920.

(29) Aagaard, L.; Laible, G.; Selenko, P.; Schmid, M.; Dorn, R.; Schotta, G.; Kuhfittig, S.; Wolf, A.; Lebersorger, A.; Singh, P. B.; Reuter, G.; Jenuwein, T. Functional mammalian homologues of the Drosophila PEV-modifier Su(var)3−9 encode centromere-associated proteins which complex with the heterochromatin component M31. *EMBO J.* **1999**, *18*, 1923−1938.

(30) Raurell-Vila, H.; Bosch-Presegue, L.; Gonzalez, J.; Kane-Goldsmith, N.; Casal, C.; Brown, J. P.; Marazuela-Duque, A.; Singh, P. B.; Serrano, L.; Vaquero, A. An HP1 isoform-specific feedback mechanism regulates Suv39h1 activity under stress conditions. *Epigenetics* **2017**, *12*, 166−175.

(31) Saha, S.; Weber, C. A.; Nousch, M.; Adame-Arana, O.; Hoege, C.; Hein, M. Y.; Osborne-Nishimura, E.; Mahamid, J.; Jahnel, M.; Jawerth, L.; Pozniakovski, A.; Eckmann, C. R.; Jülicher, F.; Hyman, A. A. Polar Positioning of Phase-Separated Liquid Compartments in Cells Regulated by an mRNA Competition Mechanism. *Cell* **2016**, *166*, 1572−1584.

(32) Brochard, F.; de Gennes, P. Collapse of one polymer coil in a mixture of solvents. *Ferroelectrics* **1980**, *30*, 33−47.

(33) de Gennes, P. *Scaling Concepts in Polymer Physics*; Cornell University Press: Ithaca/London, 1979.

(34) Wang, R.; Wang, Z.-G. Theory of Polymers in Poor Solvent: Phase Equilibrium and Nucleation Behavior. *Macromolecules* **2012**, *45*, 6266−6271.

(35) Cremer, T.; Cremer, M.; Hübner, B.; Strickfaden, H.; Smeets, D.; Popken, J.; Sterr, M.; Markaki, Y.; Rippe, K.; Cremer, C. The 4D nucleome: Evidence for a dynamic nuclear landscape based on co-aligned active and inactive nuclear compartments. *FEBS Lett.* **2015**, *589*, 2931−2943.
(36) Maeshima, K.; Rogge, R.; Tamura, S.; Joti, Y.; Hikima, T.; Szerlong, H.; Krause, C.; Herman, J.; Seidel, E.; DeLuca, J.; Ishikawa, T.; Hansen, J. C. Nucleosomal arrays self-assemble into supramolecular globular structures lacking 30-nm fibers. *EMBO J.* **2016**, *35*, 1115−1132.
(37) Gibson, B. A.; Doolittle, L. K.; Schneider, M. W. G.; Jensen, L. E.; Gamarra, N.; Henry, L.; Gerlich, D. W.; Redding, S.; Rosen, M. K. Organization of Chromatin by Intrinsic and Regulated Phase Separation. *Cell* **2019**, *179*, 470−484.
(38) Strickfaden, H.; Tolsma, T. O.; Sharma, A.; Underhill, D. A.; Hansen, J. C.; Hendzel, M. J. Condensed Chromatin Behaves like a Solid on the Mesoscale In Vitro and in Living Cells. *Cell* **2020**, *183*, 1772−1784.
(39) Bajpai, G.; Pavlov, D. A.; Lorber, D.; Volk, T.; Safran, S. Mesoscale phase separation of chromatin in the nucleus. *eLife* **2021**, *10*, No. e63976.
(40) Amiad-Pavlov, D.; Lorber, D.; Bajpai, G.; Reuveny, A.; Roncato, F.; Alon, R.; Safran, S.; Volk, T. Live imaging of chromatin distribution reveals novel principles of nuclear architecture and chromatin compartmentalization. *Sci. Adv.* **2021**, *7*, No. eabf6251.
(41) Farr, S. E.; Woods, E. J.; Joseph, J. A.; Garaizar, A.; Collepardo-Guevara, R. Nucleosome plasticity is a critical element of chromatin liquid−liquid phase separation and multivalent nucleosome interactions. *Nat. Commun.* **2021**, *12*, 2883.
(42) Galuschko, A.; Sommer, J.-U. Co-Nonsolvency Response of a Polymer Brush: A Molecular Dynamics Study. *Macromolecules* **2019**, *52*, 4120−4130.
(43) Watanabe, H.; Ito, N.; Hu, C.-K. Phase diagram and universality of the Lennard-Jones gas-liquid system. *J. Chem. Phys.* **2012**, *136*, 204102.
(44) Plimpton, S. Fast Parallel Algorithms for Short-Range Molecular Dynamics. *J. Comput. Phys.* **1995**, *117*, 1.
(45) Sommer, J.-U. Gluonic and Regulatory Solvents: A Paradigm for Tunable Phase Segregation in Polymers. *Macromolecules* **2018**, *51*, 3066−3074.
(46) Sandholtz, S. H.; MacPherson, Q.; Spakowitz, A. J. Physical modeling of the heritability and maintenance of epigenetic modifications. *Proc. Natl. Acad. Sci. U. S. A.* **2020**, *117*, 20423−20429.
(47) Winnik, F.; Ringsdorf, H.; Venzmer, J. Methanol-Water as a Co-nonsolvent System for Poly(N-isopropylacrylamide). *Macromolecules* **1990**, *23*, 2415−2416.
(48) Scherzinger, C.; Schwarz, A.; Bardow, A.; Leonhard, K.; Richtering, W. Cononsolvency of poly-N-isopropyl acrylamide (PNIPAM): Microgels versus linear chains and macrogels. *Curr. Opin. Colloid Interface Sci.* **2014**, *19*, 84−94.
(49) Mukherji, D.; Marques, C. M.; Kremer, K. Polymer collapse in miscible good solvents is a generic phenomenon driven by preferential adsorption. *Nat. Commun.* **2014**, *5*, 4882.
(50) Sommer, J.-U. Adsorption-Attraction Model for Co-Non-solvency in Polymer Brushes. *Macromolecules* **2017**, *50*, 2219−2228.
(51) Keenen, M. M.; Brown, D.; Brennan, L. D.; Renger, R.; Khoo, H.; Carlson, C. R.; Huang, B.; Grill, S. W.; Narlikar, G. J.; Redding, S. HP1 proteins compact DNA into mechanically and positionally stable phase separated domains. *eLife* **2021**, *10* DOI: 10.7554/eLife.64563.
(52) MacPherson, Q.; Beltran, B.; Spakowitz, A. J. Bottom-up modeling of chromatin segregation due to epigenetic modifications. *Proc. Natl. Acad. Sci. U. S. A.* **2018**, *115*, 12739−12744.
(53) Eeftens, J. M.; Kapoor, M.; Michieletto, D.; Brangwynne, C. P. Polycomb condensates can promote epigenetic marks but are not required for sustained chromatin compaction. *Nat. Commun.* **2021**, *12*, 5888.
(54) Yong, H.; Bittrich, E.; Uhlmann, P.; Fery, A.; Sommer, J.-U. Co-Nonsolvency Transition of Poly(N-isopropylacrylamide) Brushes in a Series of Binary Mixtures. *Macromolecules* **2019**, *52*, 6285−6293.

https://doi.org/10.1021/acs.macromol.2c00244
Macromolecules 2022, 55, 4841−4851